RSC Advances

ROYAL SOCIETY OF CHEMISTRY

www.rsc.org/advances

RSC advances

ARTICLE

Manganese oxide - an excellent microwave-induced absorbent for its oxidation of methylene blue

Received 00th January 20xx,
Accepted 00th January 20xx

DOI: 10.1039/x0xx00000x

www.rsc.org/

Xiaoyu Wang[a], Guocheng Lv[a,*], Libing Liao[a,*], Guangsheng Wang[b]

Microwave-induced oxidation is an effective method for degradation of organic pollutants with high-concentrations in wastewater. In this study, manganese oxide (MO), a mixture of 74% akhtenskite and 26% ramsdellite was used as an oxidant for microwave-induced oxidation of methylene blue (MB). With 0.1 g of MO and 2.5 mg MB, the MB removal efficiency was about 99% under 10 min microwave irradiation (MI). Oxidative capacity of MO in this study was closely related with the concentration of H^+. A strong acidic condition was optimal for MB degradation in the presence or absence of MI. The intermediates of MB degradation from $C_{16}H_{18}N_3S$ to $C_{14}H_{13}N_2OS$, $C_{13}H_{11}N_2OS$, and $C_{12}H_9N_2OS$ were identified by LC-MS. Network analysis described the excellent microwave adsorption property of MO which was mainly attributed to its dielectric loss. The maximal microwave reflection loss was about -21.23 dB for a sample that is made of 70% MO and 30% paraffin with a thickness of 6 mm. DOS calculation showed that the unit cell of akhtenskite with two manganese ions had the natural spin magnetic moment (2*Integrated Spin Density) of 6.0 which is in accordance with the theoretical calculation of two Mn^{4+} which could help the hysteresis loss under microwave. Considering the variable valence of MO and its zero electric dipole moment, it was deduced that charge transfer was the main mechanism for causing the dielectric loss.

[a] *Beijing Key Laboratory of Materials Utilization of Nonmetallic Minerals and Solid Wastes, National Laboratory of Mineral Materials, School of Materials Science and Technology, China University of Geosciences, Beijing, 100083, China*

[b] *Key Laboratory of Bio-Inspired Smart Interfacial Science and Technology of Ministry of Education, School of Chemistry and Environment, Beihang University, Beijing, 10091, China*

Electronic Supplementary Information (ESI) available: [details of any supplementary information available should be included here]. See DOI: 10.1039/x0xx00000x

The abstract should be a single paragraph that summarises the content of the article

Introduction

Microwave-induced oxidation has attracted the worldwide attention as a green technology for the treatment of organic pollutants. Under microwave irradiation (MI), degradation of organic pollutants could reach high efficiency in several minutes by microwave oxidant.[1,2] In the presence of MI, microwave-absorbing materials would release great amounts of heat and produce the reactive center, contributing to the degradation of organic pollutants.[3-5] Thus, microwave absorption ability of the oxidant is the key factor for degrading organic pollutants.

Manganese oxides (MOs) are excellent microwave absorbing materials, providing a significant oxidation capacity under MI.[6,7] Their crystal structures are usually constituted by [MnO_6] octahedra linked by edge-sharing or corner-sharing, which could be described by edge connected octahedral chains sharing corners or edges to generate tunnel or layered structures.[8] MOs are usually divided into several types of crystal structure (Fig. 1), such as pyrolusite group described as [1×1] tunnel structure with single octahedral chains connected by corner-sharing (Fig. 1a), ramsdellite group described as [1×2] tunnel structure with single and double octahedral chains connected by corner-sharing (Fig. 1b), hollandite group described as [2×2] tunnel structure with double octahedral chains connected by corner-sharing (Fig. 1c), romanechite group described as [2×3] tunnel structure with double and three octahedral chains connected by corner-sharing (Fig. 1d), todorokite group described as [3×3] tunnel structure with three octahedral chains connected by corner-sharing (Fig. 1e), birnessite group described as [1×∞] layered structure with single or multi-chains connected by edge-sharing (Fig. 1f), akhtenskite described with hexagonal close packing structure (Fig. 1g) and spinel structure (Fig. 1h).[9,10]

When exchangeable cations are present in tunnels or layers, substitution of Mn^{4+} by Mn^{3+} or Mn^{2+} occurred to balance the residual positive charge during the generation of MOs.[11,12] MOs with variable valences have better electromagnetic properties under MI by accelerating the dielectric loss between Mn^{4+} and Mn^{3+} or Mn^{2+} than those with single valence.[13,14]

Previous studies on microwave-induced oxidation were focused on degradation efficiency and reaction conditions,[2,15-18] fewer involved in the crystal structural details to address the mechanisms of microwave-induced oxidation by MOs. In this work, MOs were used as microwave oxidant to degrade methylene blue (MB) in water. The removal efficiency, pH condition, reaction process, and reaction mechanism were discussed. Based on the relationship between structure details and oxidant property, a new type of microwave-induced oxidation integrating degradation and adsorption was designed to treat organic pollutants.

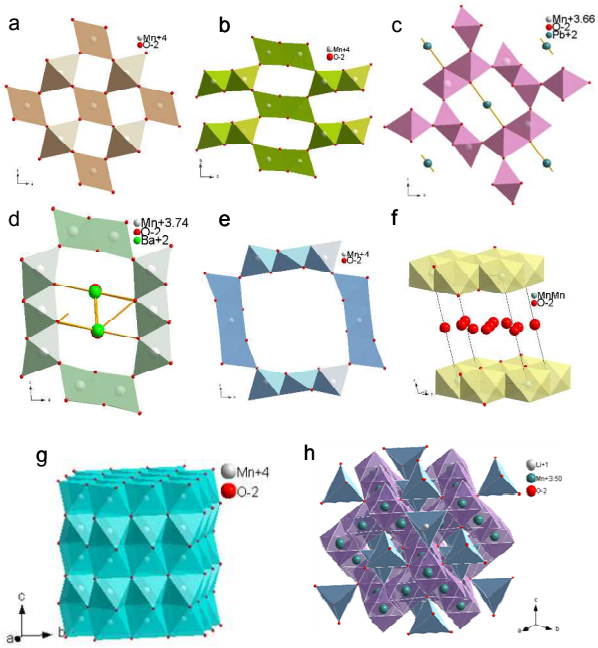

Fig. 1 Crystal models of different manganese oxides. (a) Pyrolusite with [1×1] tunnel structure. (b) Ramsdellite with [1×2] tunnel structure. (c) Hollandite with [2×2] tunnel structure. (d) Romanechite with [2×3] tunnel structure. (e) Todorkite with [3×3] tunnel structure. (f) Birnessite with [1×∞] layered structure. (g) Akhtenskite

with hexagonal close packing structure and (h) spinel structure.

Materials and methods

Materials

MO used was provided by Beijing Kang Puhui Technology Company with a formula weight of 86.94 g/mol, a melt point of 535 °C and appeared to be powder in brownish black. MB used was supplied by Beijing Chemical Works with the molecular formula of $C_{16}H_{24}N_3S$ and formula weight of 284 g/mol (in solution) which usually presents a crystal powder in dark green, and can easily be dissolved by water to form a dark blue solution. All chemicals were of analytical grade, and were used as received without further purification. All aqueous solutions were prepared in distilled water.

Methods

In all batch experiments, 0.1 g MO was added to 25 mL of 100 mg/L MB solutions for the time series study and 25 mL of 120 mg/L for the pH study. The pH was controlled by adding minimum amounts of 0.01 M HCl or 0.01M NaOH solutions. The microwave (Tangshan nano microwave thermal instrument manufacturing co., LTD) power was set at 700 W. The reaction time was at 1, 2, 3, 4, 5, 6, 7, 8, 9, and 10 min, and the pH was from 1 to 11 at intervals of 2. After reaction, the slurry was centrifuged at 7500 rpm for 3 min, then filtered with a 0.25 μm syringe-type filter to a 50 mL tube for Ultraviolet-visible (Uv-vis) and Liquid Chromatograph-Mass Spectrometer (LC-MS) analysis.

Instrumentation

Crystal structure of MO for each treatment was determined by a Powder X-Ray Diffraction (PXRD, BRUKER) with Cu Ka-radiation in step width of 0.02° from 2Th of 5□ to 80□. Valence of irons on surface of raw MO was confirmed by X-ray Photoelectron Spectroscopy (XPS, Thermo Scientific) with monochromatic of 150W AlKα irradiation. Elemental composition of MO was determined by X-Ray Fluorescence spectrometry (XRF, Beijing North Early Microstructure Analysis and Test Center Co., Ltd.). Degradation efficiency of MB was calculated on the basis of standard curve at the maximum absorbing wavelength of 665 nm using a UV765 Uv-vis spectrophotometer (Shanghai Precision Scientific Instrument Co., Ltd.). Residual MB and its degradation intermediates were measured by LC-MS (Thermo Scientific). Microwave absorbing property of MO was investigated using a network analyzer instrument (Thermo Scientific Co., Ltd.) from 2 to 18 GHz. During the network analysis, the samples were mixed with paraffin to different mass ratios and the mass percent was calculated by dividing the mass of MO by the total mass. Density of state (DOS) curve of akhtenskite were performed by Material studio CASTEP model (Ms, Accelrys) in functional of GGA and WC with energy of 500 eV.

Results and discussion

Characterization

MO used in this study was a mixture of 74% akhtenskite and 26% ramsdellite characterized by Rietveld fit to the PXRD pattern (Fig. 2a). This is comparable with the result of Chang-Hoon Kim et al.[19] Full width at the half maxi mum (FWHM) reflected the poor crystallization of ramsdellite. Akhtenskite was a hexagonal close packing structure with the space group of $P6_3/mmc$ and cell parameters of a=2.777(2) Å, c=4.424(9) Å, and V=29.66(2) $Å^3$ with an approximate formula of MnO_2,[5,19] which is favored in oxidation application.[20] Traditionally, cations could hardly be absorbed into akhtenskite due to its hexagonal close packing structure. In contrast, ramsdellite has a [1×2] tunnel structure with the space group of Pnam and cell parameters of a=8.555(2) Å, b=4.415(4) Å, and c=2.857(9) Å in which cations could be absorbed into its tunnels to balance the residual negative charges caused by substitution of Mn^{4+} by Mn^{3+} or Mn^{2+}.[11] XPS analysis showed the main elements were Mn, O, Na and C,

confirming that Na was the main cation in ramsdellite tunnels (Fig. 2b). Element analysis showed that O and Mn accounted for 96 %, confirming that MO was the major component with some adsorbed cations of Na, K and impurity elements of C and N (Table 1).

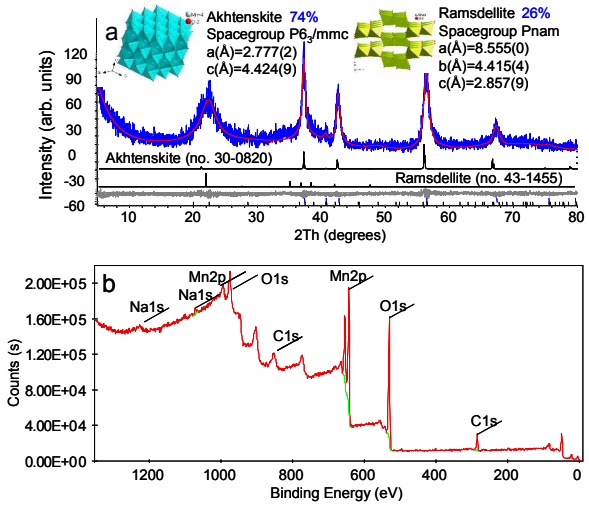

Fig. 2 XRD and XPS patterns of MO. (a) The Rietveld analysis suggests that MO consists of 74% Akhtenskite and 26% Ramsdellite. (b) XPS analysis showed that variable valences were present in MO.

Table. 1 Elemental analysis of MO.

Components	Results (mass%)	Detection limit (mass%)	Spectral Lines
C	0.32	0.02992	C-K α
N	0.374	0.06182	N-K α
O	40.6	0.10627	O-K α
Na	0.224	0.00593	Na-K α
Al	0.134	0.00131	Al-K α
K	0.057	0.00105	K-K α
Mn	55.4	0.00749	Mn-K α
Total	99.05		

Removal efficiency of MB by MO under natural acidity in the presence or absence of MI

Investigation on degradation of MB exposed at MI (MI/MB), MO (MO/MB), MO and MI (MI/MO/MB) were first determined. Fig. 3a showed the Uv-vis spectrum of reaction products in above systems with different reaction time at wavelength from 500 nm to 700 nm. Lower absorbance indicated the lower residual concentration and higher removal efficiency of MB. Results showed that compared with raw MB (100 mg/L), the spectrum in the system of MI/MB remained essentially same with that of raw MB, suggesting no removal or degradation of MB by dissolved oxygen under MI in 100 °C. The maximum absorption peak of MB at 665 nm in both system of MO/MB and MI/MO/MB decreased gradually with time and the absorbance at 665 nm in system of MI/MO/MB were lower than that in the system of MO/MB, indicating higher MB removal efficiency in the system of MI/MO/MB. In the system of MO/MB, the maximum absorption peak at 665 nm decreased with time and the peak profiles preserve uniformly as compared to that of the raw MB. Equilibrium time was about 10 min in this system, so the main reaction was possible an adsorption process. In the system of MI/MO/MB, the absorption peak at 665 nm gradually disappeared and the peak at 600 nm became the new maximum absorption peak, suggesting degradation of MB with time and appearance of reaction intermediates.

The removal efficiency η was calculated by $\eta=100(1-C_t/C_0)\%$, where C_0 and C_t are the initial and residual MB concentrations at time t (mg/L). The removal efficiency of MB in the system of MI/MB were almost zero at any time, indicating that MB could not be degraded by the residual oxygen in air and water even induced by microwave (Fig. 3b). The removal efficiency of MO/MB in water could reach to about 48% in 10 min. In contrast, the removal efficiency of MB increased significantly with time and reached 99.5% in 10 min in the presence of MI. The excellent response between MO and microwave would result in dual effects of adsorption and oxidation.

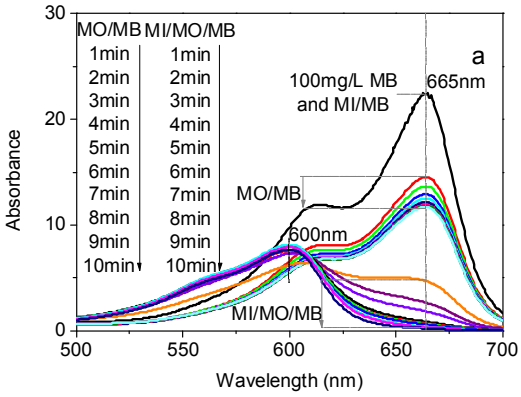

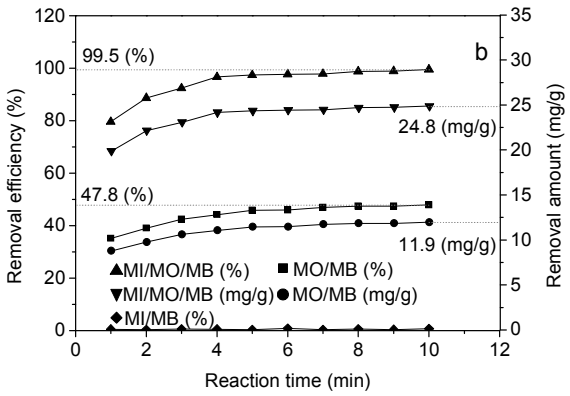

Fig. 3 Removal efficiency of MB by MO under natural acidity in the presence and absence of MI. (a) Full spectrum of reaction supernatant in systems of MI/MB, MO/MB and MI/MO/MB. (b) Removal efficiency of MB with time as measured by absorbance at 665 nm in the systems of MI/MB, MO/MB, and MI/MO/MB.

LC-MS of MB and its products formulas

Using high resolution search the molecular formula of residual products in the system of MI/MO/MB were $C_{14}H_{13}N_2OS$, $C_{13}H_{11}N_2OS$, and $C_{12}H_9N_2OS$ after 1 min and $C_{12}H_9N_2OS$ after 10 min MI (Fig. 4), implying a gradual process of degradation from MB to $C_{14}H_{13}N_2OS$, $C_{13}H_{11}N_2OS$ and $C_{12}H_9N_2OS$. Actually, the temperature of MnO_2 could rise up to about 1000 °C by MI in 100 s.[21,22] Thus, high temperature accounted for the oxidation of MB by MO.

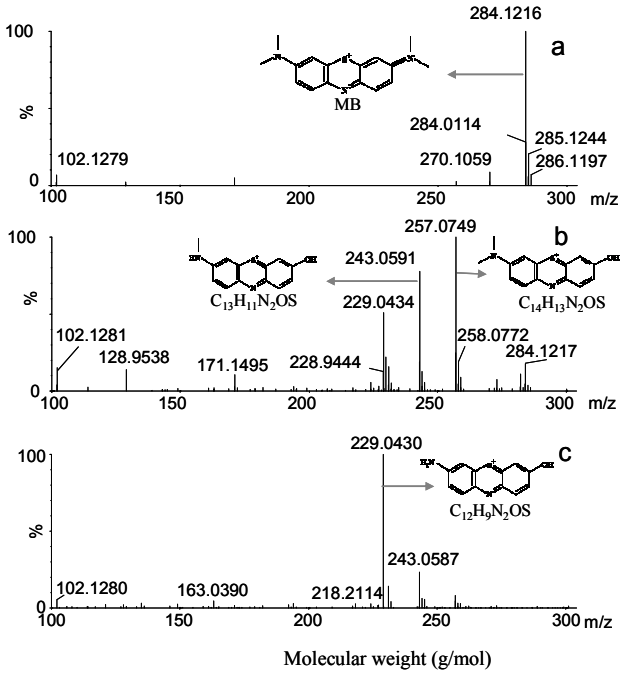

Fig. 4 LC-MS identification of MB (a) and its degradation products under MI/MO for 1 min (b), 10 min (c).

Effects of reaction pH on MB degradation efficiency

To investigate the effects of pH on MB degradation efficiency, standard curves at different pH were determined to calculate the removal efficiency more accurately. Results showed that the maximum absorption peak of MB at different pH were all at 665 nm by Uv-vis, but different peak intensities displayed in different pH (Fig. 5a). With the increase of pH, the peak intensity of full spectrum from 500 to 700 nm decreased gradually. The full spectra of concentrations at 2, 4, 6, 8, and 10 mg/L at pH from 1 to 11 were not overlapped, showing an intensity gradient at different MB concentrations.

Based on the absorbance at 665 nm, several standard curves at pH from 1 to 11 were made. The slope of the standard curves decreased gradually with the increase of pH, prompting a gradually reduction of absorbance at 665 nm with the same concentration. The calibration equations of MB at pH of 1, 3, 5, 7, 9 and 11 were y=0.2188x-0.121, y=0.2155x-0.1763, y=0.211x-0.1865, y=0.202x-0.1886, y=0.1971x-0.201 and y=0.1674x-0.1345, respectively, with the R^2 values all above 0.95 (Fig. 5b).

After 10 min reaction in the systems of MO/MB and MI/MO/MB at different pH, the absorbance values of the system of MI/MO/MB at 665 nm were all lower than those of MO/MB in pH from 1 to 11 (Fig. 5c), implying a higher MB removal efficiency in the presence of MI. In the system of MO/MB, during the higher oxidation under a strong acidic condition, the maximum absorption wavelengths of products were lower than 665 nm when the pH condition declined to 1 and 3. Particularly, significant offset of maximum absorption peak occurred at pH 1 with the lowest absorbance at 665 nm than others. Secondly, offset of maximum absorption peak occurred at pH of 3 which led to the lower absorbance at 665 nm than that at pH 5. In the residual pH conditions from 5 to 11, absorbance of full spectrum of products decreased gradually with the increase of pH. In the system of MI/MO/MB, all the maximum absorption wavelengths of products shifted to about 600 nm, confirmed the degradation of MB in 10 min under MI. Among them, the full spectrum absorbance reached the lowest value at pH 1. In residual pH conditions from 3 to 11, absorbance of full spectrum of products decreased gradually with the increase of pH.

Based on the absorbance at 665 nm in the systems of MI/MO/MB and MO/MB (Fig. 5c) and the standard curve equations (Fig. 5b), the MB removal efficiencies at different pH conditions at 665 nm were calculated (Fig. 5d). Maximum MB removal efficiency in the system of MI/MO/MB and MO/MB occurred both under a strong acidic condition even calculated by higher slope in standard equations, suggesting that strong acid could enhance the oxidation of MO and increase the MB removal efficiency. The half reaction of MnO_2 was $MnO_2+4H^++2e^- \rightarrow Mn^{2+}+2H_2O$, and similarly, the half reaction of MnO_x was $MnO_x+2xH^++(2x-2)e^- \rightarrow Mn^{2+}+xH_2O$. Thus, oxidative capacity of MO in this study was closely related with the concentration of H^+. When the pH values declined, the concentration of H^+ increased exponentially. Thus, the reaction was more effective under strong acidic pH condition. In neutral and alkaline conditions, the change in H^+ concentration was relatively small and the oxidative capacity of MO was stable.

After MI at different pH, XRD patterns of MO before and after reaction were comparable with those of raw MO which demonstrated no structural damage after MI (Fig. 5e) .

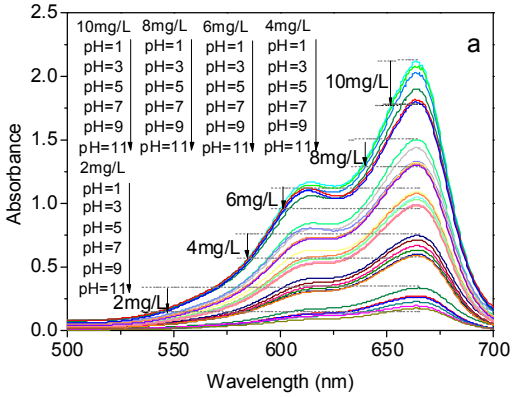

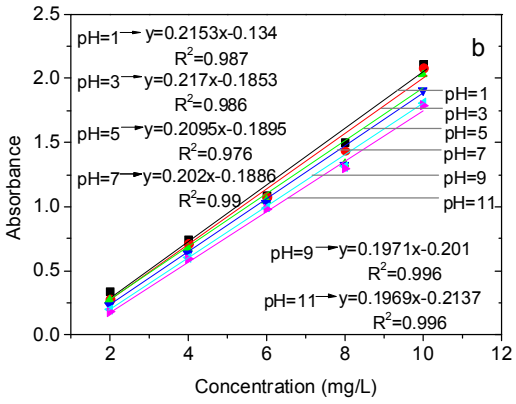

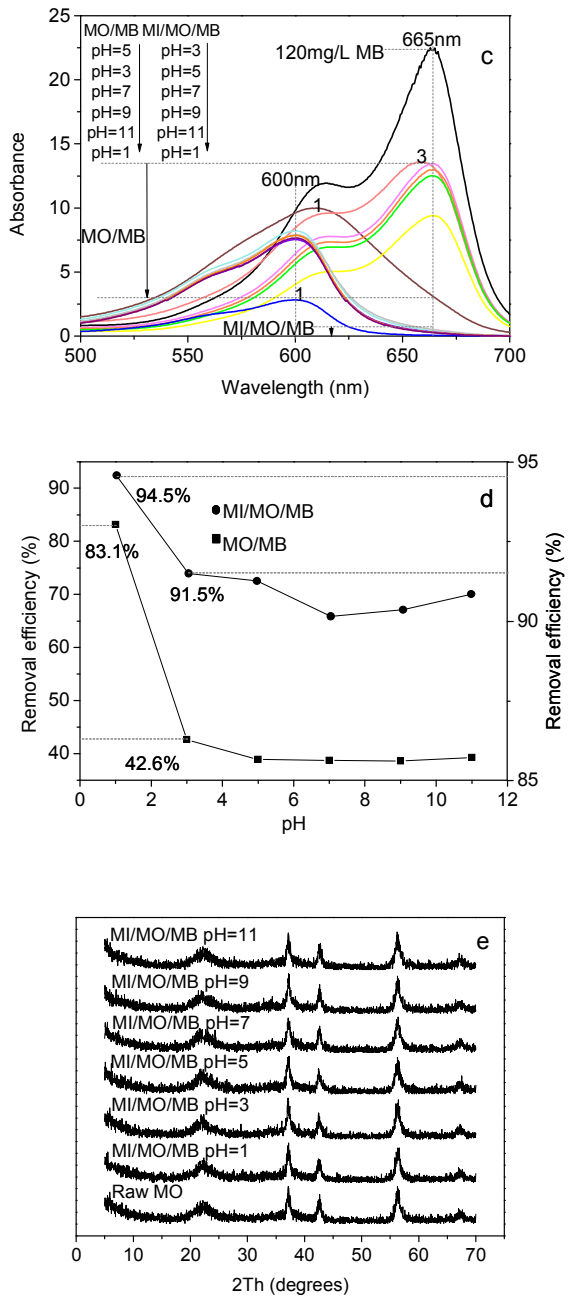

Fig. 5 Effects of pH on MB degradation efficiency and XRD patterns of MO before and after reaction at different pH. (a) Full spectra of concentrations of 2, 4, 6, 8, and 10 mg/L at pH range from 1 to 11. (b) Standard curves at pH from 1 to 11. (c) Full spectra of reaction products in the systems of MO/MB and MI/MO/MB at different pH. (d) Effects of pH on MB removal efficiency by MO in the presence or absence of MI. (e) XRD patterns of MO before and after reaction at different pH.

Network analysis of MO

In this type of experiments, paraffin was added as the matrix and adhesive to form the plastic sample for generating a hollow cylinder. Network analysis showed that MO has an excellent microwave absorbing property at the range from 2 to 18 GHz, which was attributed to both dielectric loss and hysteresis loss. What's more, the tangent value of the hysteresis loss and dielectric loss increased as the mass percentage of MO. Among them, the tangent value of dielectric loss increased from about 0.04 to 0.3 at MO mass percent from 5% to 70% (Fig. 6a), while the tangent value of hysteresis loss increased from about 0.08 to 0.12 at MO mass percent from 5% to 70% (Fig. 6b). Thus, dielectric loss was the main factor in the microwave adsorption. As higher mass percent, samples could represent electromagnetic property more accurately. Thus, samples with mass percent of 70% could reflect the electromagnetic property of MO better. The maximal reflection loss (RL) values for the samples of 50 and 70% MO mass were -12.56 and -21.23 dB, respectively (Fig. 6c-d). Particularly, at the coating thickness above 3 mm, the maximal RL values of the sample with 70% MO mass were all above -10 dB and the optimal RL value was about -21.23 dB in the thickness of 6 mm, implying the excellent microwave adsorption property of MO (Fig. 6d).

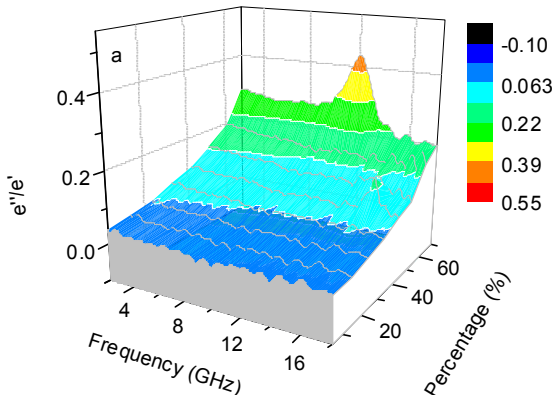

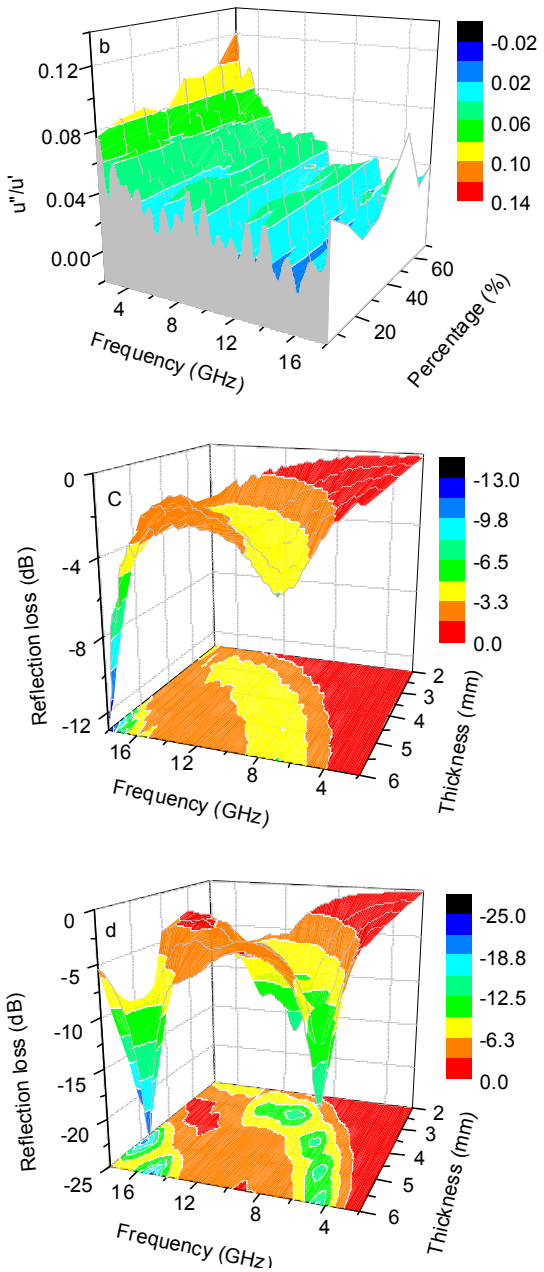

Fig. 6 Network analysis of MO. (a) Tangent value of dielectric loss with mass percent from 5 to 70%. (b) Tangent value of hysteresis loss with mass percent from 5 to 70%. (c) Reflection loss of a sample with 50% MO mass. (d) Reflection loss of a sample with 70% MO mass.

DOS calculation

As the MO was a mixture mainly made of akhtenskite, DOS calculation was made on akhtenskite by Material studio with the CASTEP model. In the weaker coordination environment of O, the 3d electrons of Mn and Co would be present in a high spin state, leading to the spin-polarized electrons of 5, 4, and 3, respectively in single Mn^{2+}, Mn^{3+}, and Mn^{4+}. The ideal natural spin magnetic moment of the unit cell of akhtenskite with two manganese irons was 6 (calculated as 2*Integrated Spin Density), which was in accordance with the theoretical calculation of two Mn^{4+} (Fig. 7). Thus, natural spin magnetic moments present in the crystal lattice of $[MnO_6]$ octahedral. The electronic configurations of Mn^{3+} and Mn^{4+} were $3d^4$ and $3d^3$, respectively. Both have natural spin magnetic moment, forcing the hysteresis loss under MI. This piece of information suggested that natural spin magnetic moment of the center Mn was the main role for producing hysteresis loss and quick heating under MI.

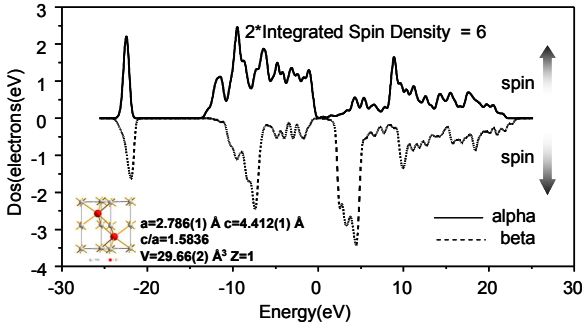

Fig. 7 DOS calculation of unit cell of akhtenskite.

Space group of Akhtenskite and ramsdellite are $P6_3/mmc$ and Pnam, which both have the centrosymmetric structure with zero electric dipole moment in theory.[5] Thus, the dielectric loss caused by the permanent electric dipole moment was minute. Electron transfer enhanced the oxidation activity of MnO_2.[23,24] As such, it is probable that charge transfer is the main reason for causing the dielectric loss. MO used in this work was a mixture of akhtenskite and ramsdellite with [1×2] tunnel structure. For the latter, there were variable valences of Mn in the $[MnO_6]$ octahedra. Thus, under the high frequency variation of alternating electromagnetic field, manganese ions in adjacent octahedra could transfer electrons and exchange valances, causing the dielectric loss in MO, which could

lead to the dielectric loss of the system and converting microwave energy into heat energy, that will produce the reactive center and reduce the activation energy and contributed to the overall reactivity. Thus, it was deduced that natural spin magnetic moment of the center Mn was the main role for producing hysteresis loss and charge transfer was the main cause for the dielectric loss under MI.

To sum up, the spectrum in the system of MI/MB was basically consistent comparing with that of raw MB, suggesting no removal or degradation of MB by dissolved oxygen even under MI in 100 °C. In contrast, under MI or in a strong acidic condition, the absorbance at 665 nm gradually disappeared and the peak at about 600 nm became the new maximum, suggesting degradation of MB under MI or in a strong acidic condition and MO acted as an oxidant. On the surface of MO under MI, high temperature accounted for the oxidation of MB by MO. Thus, oxidation of MB by MO occurred on the surface of MO by MI and no removal or degradation of MB by dissolved oxygen was found even under MI in 100 °C (Fig. 8).

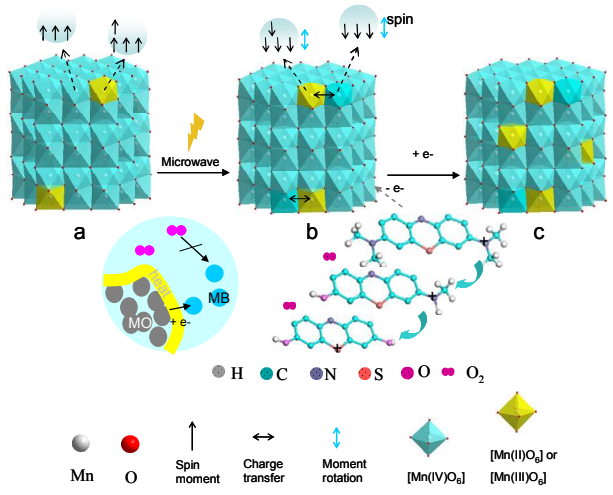

Fig. 8 Mechanism of microwave-induced oxidation of MB. in the presence of MO, using akhtenskite as the model crystal. Under natural conditions, the spin directions are the same (a). In the presence of MI, the spin directions alternate (b). In the presence of reductant (MB in this case), some of the Mn^{4+} were reduced to Mn^{2+} or Mn^{3+} (b to c).

Conclusions

In the presence of the microwave oxidant MO, the degradation of MB under MI was superior to that without MI and the optimal pH environment was at a strong acidic condition due to the high concentration of H^+. Sequential process of MB degradation was verified by LC-MS from $C_{16}H_{18}N_3S$ to $C_{14}H_{13}N_2OS$, $C_{13}H_{11}N_2OS$, $C_{12}H_9N_2OS$ Thus, MO acted as the adsorbent and microwave-induced oxidant. Electromagnetic network analysis showed that both dielectric loss and hysteresis loss contributed to microwave induction. Natural spin magnetic moment of the center Mn was the main role for producing the hysteresis loss. Adjacent Mn of different valences in octahedra would promote the high frequency electron transfer under microwave, which could produce significant dielectric loss. So, it was deduced that charge transfer was the reason for causing the dielectric loss. Thus, MO which has more variable valences and higher spin magnetic moment possibly has better response in MI for treating organic pollutants.

Acknowledgments

We thank M. L. Qiu and Y. Tian for their assistance in XRF and LC-MS measurements, as well as C.C. Zhao for DOS calculation. This project was supported by Beijing Municipal Natural Science Foundation (No. 2153041) and Beijing Higher Education Young Elite Teacher Project (No. YETP0634).

References

1. Y. B. Zhang, X. Quan, S. Chen, Y. Z. Zhao, F. L. Yang, Journal of Hazardous Materials. B137 (2006) 534–540.

2. T. Lai, K. F. Yong, J. W. Yu, J. H. Chen, Y. Shu, C. B. Wang, Journal of Hazardous Materials. 185 (2011) 366-372.
3. H. Wang, Y. Wu, Z. W. Liu, L. He, Z. Y. Yao, W Y. Zhao, Fuel. 136 (2014) 185-193.
4. O. S. Nuri, A. Mehdilo, M. Irannajad, Applied Surface Science. 311 (2014) 27–32.
5. X. Y. Wang, L. F. Mei, X. B. Xing, L. B. Liao, G. C. Lv, Z. H. Li, L.M. Wu, Applied catalysis B-environmental. 160 (2014) 211-216.
6. E. Vileno, H. Zhou, Q. H. Zhang, S. L. Suib, D. R. Corbin, T. A. Koch, Original Research Article Journal of Catalysis. 187 (1999) 285-297.
7. A. Bello, O. O. Fashedemi, M. Fabiane, J. N. Lekitima, K. I. Ozoemena, N. Manyala, Electrochimica Acta. 114 (2013) 48-53.
8. S. Ching, J. P. Franklin, C. M. Spencer, Polyhedron. 58 (2013) 53-59.
9. M. Sakao, N. Kijima, J. Akimoto, T. Okutani, Solid State Ionics. 243 (2013) 22-29.
10. O. Ghodbane, J. L. Pascal, F. Favier, ACS Applied materials interfaces. 1 (2009) 1130-1139.
11. X. Zhang, P. Yu, H. T. Zhang, D. C. Zhang, X. Z. Sun, Yanwei Ma, Electrochimica Acta. 89 (2013) 523-529.
12. X. Zhang, X. Z. sun, H. T. Zhang, C. Li, Yanwei Ma, Electrochimica Acta. 132 (2014) 315-322.
13. S. K. Meher, G. R. Rao, Journal of Power Sources. 215 (2012) 317-328.
14. G. P. Xiong, K.P.S.S. Hembram, R.G. Reifenberger, T. S. Fisher, Journal of Power Sources. 227 (2013) 254-259.
15. H. M. Chen, P. K. Chu, J. H. He, T. Hu, Journal of Colloid and Interface Science. 359 (2011) 68-74.
16. Y. S. Wu, X. L. Yin, S. T. Xing, Z. C. Ma, Y. Z. Gao, L. Feng, Materials Letters. 110 (2013) 16-19.
17. Z. H. Lian, F. D. Liu, H. He, X. Y. Shi, J. S. Mo, Z. B. Wu, Chemical Engineering Journal. 250 (2014) 390-398.
18. W. C. Zhan, X. Y. Zhang, Y.L. Guo, L. Wang, Y. Guo, G. Z. Lv, Journal of rare earths. 32 (2014) 146.
19. C. H. Kim, Z. Akasea, L.C. Zhang, A. H. Heuer, A. E. Newman, P. J. Hughes, Journal of Solid State Chemistry. 179 (2006) 753-774.
20. R. B. Valim, M. C. Santos, M. R. V. Lanza, S. A. S. Machado, F. H. B. Lima, M.L. Calegaro, Electrochimica Acta. 85 (2012) 423–431.
21. J. Chen, P. F. Tian, X. A. Song, N. Li, J. X. Zhou, Journal of Iron and Steel Research International. 17(3) (2010) 13-20.
22. H. T. Guan, G. Chen, S. B. Zhang, Y. D. Wang, Materials Chemistry and Physics. 124(1) (2010) 639-645.
23. C. Shi, G. L. Zang, Z. Zhang, G. P. Sheng, Y. X. Huang, G. X. Zhao, X. K Wang, H. Q. Yu, Electrochimica Acta . 132 (2014) 239-243.
24. D. D. Han, X. Y. Jing, P. C. Xu, Y. S. Ding, J. Y. Liu, Journal of Solid State Chemistry 218 (2014) 178–183.